PAPER

Interferometry of binary stars using polymer optical fibres

IOP Publishing European Journal of Physics
Eur. J. Phys. **38** (2017) 045704 (14pp) https://doi.org/10.1088/1361-6404/aa7038

Interferometry of binary stars using polymer optical fibres

L Arregui[1,2], M A Illarramendi[3], J Zubia[4], R Hueso[3] and A Sánchez-Lavega[3]

[1] Fundación Tekniker, Iñaki Goenaga 5, E-20600 Eibar, Spain
[2] Aula Espazio Gela, Faculty of Engineering, University of the Basque Country UPV/EHU, Alda. Urquijo s/n, E-48013 Bilbao, Spain
[3] Applied Physics Department I, Faculty of Engineering, University of the Basque Country UPV/EHU, Alda. Urquijo s/n, E-48013 Bilbao, Spain
[4] Communications Engineering Department, Faculty of Engineering, University of the Basque Country UPV/EHU, Alda. Urquijo s/n, E-48013 Bilbao, Spain

E-mail: laura.arregui@tekniker.es, ma.illarramendi@ehu.eus, joseba.zubia@ehu.eus, ricardo.hueso@ehu.eus and agustin.sanchez@ehu.eus

Received 25 January 2017, revised 6 April 2017
Accepted for publication 28 April 2017
Published 25 May 2017

Abstract

We show a laboratory experiment in which students can learn the use of interferometry as a valuable tool in astronomy. We detail experiments based on the use of the classic Michelson stellar interferometer able to reproduce the size of single stars and to characterize double star systems. Stellar sources, single and double, are reproduced by a laser light emerging from the circular end faces of one or two step-index polymer optical fibres. Light coming from the fibre end faces passes through two identical pinholes located on a lid covering the objective of a small telescope, thus producing interference fringes. The measurement of the fringe visibilities allows us to estimate both the diameters of the simulated stars and the separation between them, with errors lower than 18% for a range of light sources that can recreate the apparent size of the outer Solar System planets Uranus and Neptune and the binary properties of the Alpha Centauri system. The exercises here described illustrate the optical principles of spatial interferometry and can be integrated into courses on astronomy, optics or space science, with close interaction between theory and experiment.

Keywords: spacial interferometry, optics, fibre, stellar diameters, interferometer

(Some figures may appear in colour only in the online journal)

1. Introduction

For centuries, astronomers have relied on increasing their telescope diameters in order to detect faint objects and improve the spatial resolution of their observations. The bigger the aperture of the telescope, the smaller the size of the Airy disc limiting the spatial resolution and the higher the collected irradiance levels [1]. For ground-based telescopes, the image resolution also depends on the turbulent motion of the Earth's atmosphere. To correct this effect, adaptive optics [2] that correct distortions of the wavefront introduced by the atmosphere, and other techniques, such as the 'lucky imaging' method [3, 4] that is based in high-speed observations that are able to effectively freeze the distorting effects of turbulence in the atmosphere, are required.

Still, when the diffraction limit of a telescope is reached, most stars are so far away that they can not be resolved even with the largest telescopes available today, such as the Gran Telescopio de Canarias (GranTeCan) in Spain with a diameter of 10.4 m or the Hubble Space Telescope (HST), with a diameter of 2.4 m in Earth orbit, free of the disturbing effects of the atmosphere. Future facilities like the European Extremely Large Telescope (E-ELT) in Chile, designed to have a diameter of 39 m, and the James Web Space Telescope (JWST), designed to have a diameter of 6.5 m will beat current limits.

The angular resolution of a conventional telescope of diameter D is given by the well-known Rayleigh criterion: $1.22\lambda/D$ [1, 5]. For instance, the diffraction limit of a single telescope with a diameter of 8 m is about $0.02''$ for visible red light ($\lambda = 650$ nm). A possibility to improve over this limit is by joining individual telescopes to form a spatial interferometer where the resolution is no longer limited by an individual telescope's diameter but by the distance between different telescopes, known as the baseline. For instance, in the case of two telescopes of 8 m separated a distance of 130 m, as is the case of the Very Large Telescope Interferometer (VLTI), the spatial resolution improves by a factor of 16.

In 1890 Michelson proposed the first interferometric mechanism, nowadays known as the Michelson stellar interferometer. Three decades later, in 1920, Michelson and Pease measured the stellar diameter of the red giant Betelgeuse ($0.05''$) using this technique [6]. Because of the high spatial resolution and the multiple applications it offers, spatial interferometry is nowadays used in many astronomy fields [7]. Unfortunately, even advanced courses on optics and astronomy do not cover spatial interferometric applications due to the difficulties in experimental set-ups. Although the determination of stellar diameters using the Michelson stellar interferometer is described in most of the classic optics textbooks [1, 5] and in some specialized works [8–10], very little has been written about experimental activities related with the topic. Some examples can be found in the education research literature. For instance, Pryor developed an early simple laboratory experiment to show interference fringes from stellar-like sources [11]. Sharpe and Collins [12] described experiments aimed to demonstrate the changes in optical spatial coherence from sources of different sizes, and Koda *et al* [13] present educational experiments aimed to introduce radio interferometry principles. Alternatively, other simple laboratory experiments have been designed to teach the power of interferometry in high-precision measurements of distances [14, 15]. However, the first class of experiments often lack a connection to real astronomy or consist of complex equipment that make them unsuitable for undergraduate or postgraduate courses, while the second type are not directly connected to astronomy.

We have developed a laboratory interferometric experiment that provides the hands-on experience to understand the basic concepts underlying spatial interferometry of optical light. Our purpose is to show the principles of optical interferometry and its applications in astronomy in fields such as the determination of the size of distant light sources and the study

of multiple sources like double stars. The experiment is based on the principles of the Michelson interferometer and constitutes an extension of previous work where we simulated the emission of a single star and estimated the size of the light source [16]. In this case, we have extended the experimental set-up to be able to simulate not only single stars but also different binary stellar systems. The interferometer allows one to measure sizes and separations between different extended sources and can be built by simple equipment available in most astronomy and optics departments. The satisfactory results obtained, the simplicity of the equipment and the close connection between theory and experiment make it an ideal practice to integrate in postgraduate courses.

2. Theoretical background

An optical stellar interferometer consists of two or more telescopes which detect light emitted from a distant system, with the aim of obtaining information of the system with very high angular resolution. A simplified operation of this interferometer can be carried out by using a single telescope whose aperture is covered by a lid with two circular pinholes of variable separation between them. The optical fundamentals of this device are based on those of the Young's double-slit experiment. In this case, the beams emerging from each pinhole form interference fringes in the focal plane of the telescope. The quality of the fringes is described quantitatively in terms of the fringe visibility V, which is defined as,

$$V = \frac{I_{\max} - I_{\min}}{I_{\max} + I_{\min}} \tag{1}$$

where $I_{\max}$ and $I_{\min}$ are the maximum and minimum irradiances of the interference pattern [1].

From the theory of optical coherence [1, 5], the fringe visibility is interpreted as a measure of the degree of coherence in the two-pinhole system considering a quasi-monochromatic light coming from a spatially incoherent source. Particularly, the van Cittert–Zernke theorem describes the relationship between the irradiance distribution of the source and the corresponding fringe visibility. If the light source is described as a circular and uniform disk, which is the simplest model to describe the emission of a star, the fringe visibility is given by the following expression [5],

$$V = 2\left|\frac{J_1(\pi da/L\lambda)}{(\pi da/L\lambda)}\right| \tag{2}$$

where J_1 is the first-order Bessel function of the first kind, a the linear diameter of the source, L the distance between the two-pinhole system and the light source, d the distance between the pinholes (or baseline) and λ the light wavelength. According to (2) the visibility decreases steadily from a value of unity when $\pi ad/L\lambda = 0$ to a value of zero when $\pi ad/L\lambda = 1.22\pi$.

If the light source consists of two circular and uniform disks (1 and 2) separated by a certain distance, which could represent a binary stellar system, the corresponding fringe visibility is expressed as follows [17],

$$V = \left|\frac{V_1^2 + V_2^2 f^2 + 2f|V_1||V_2|\cos(2\pi da_s\cos\theta/L\lambda)}{(1+f)^2}\right|^{1/2}. \tag{3}$$

Here, V_1 and V_2 are the visibility functions for each disk of diameters a_1 and a_2 given in (2), f is the ratio between the the total integrated flux received from source 2 at a given wavelength, to that received from source 1, which is called the contrast of the binary system, a_s is the linear distance between disks, and θ is the angle between the imaginary line that joins

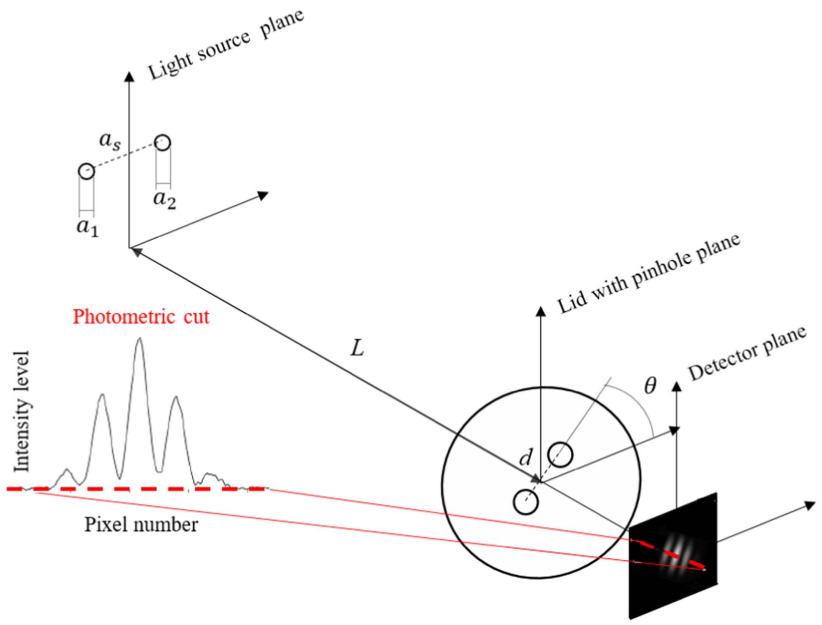

Figure 1. Diagram showing a double light source, the lid with two pinholes and the telescope's detector. A scheme of the fringes obtained is also shown. The orientation of the fringes depends on the orientation of the sources and pinholes, as explained in the text.

the centres of the two disks with respect to the line that joins the two pinholes in the telescope, see figure 1. If both disks have the same linear diameter (a) and emit the same radiance, i.e. $V_1 = V_2 \equiv V$ and $f = 1$, (3) can be simplified to the following expression,

$$V = \frac{2}{\sqrt{2}} \left| \frac{J_1(\pi da/L\lambda)}{\pi da/L\lambda} \right| \left| 1 + \cos\left(\frac{2\pi d a_s \cos\theta}{L\lambda}\right) \right|^{1/2}. \tag{4}$$

This equation expresses that the visibility produced by two identical disks is modulated by the visibility that a single disk of the same diameter a would produce. It can be easily concluded that V is zero, either if $\pi a_s d/L\lambda = (n + 1)\pi/2$ ($n = 0, 1, 2, \ldots$) in the cosine function, or if $\pi ad/L\lambda = 1.22\pi$ in the first factor, corresponding to a single disk. The minima of V due to the cosine function will only drop to 0 if the contrast f is 1. It can be shown that the amplitude of the modulation decreases as f is reduced [17].

If the distant L and the light wavelength λ are known, we can determine the diameter of the single disk a by measuring the curve of the visibility V of the fringes as a function of the baseline d and by fitting (2) to this curve [16]. Similarly, we can calculate the linear diameters of two disks together with their linear separation a_s by measuring the dependence of the visibility V of the binary system on d and by fitting (3) to the curve. Although the aforementioned procedures are the most accurate ones, in some cases there are alternative and easier procedures to determine the parameters of the light source. For the case of a single disk, the linear diameter of the source can be estimated by measuring the lowest value of d at which the interference fringes disappear, in which case $d = 1.22\lambda L/a$. For a binary system in which the two disks have the same linear diameter, $\theta = 0°$ and $f = 1$, the linear separation a_s could be estimated by measuring the lowest value of d at which the interference fringes disappear, in

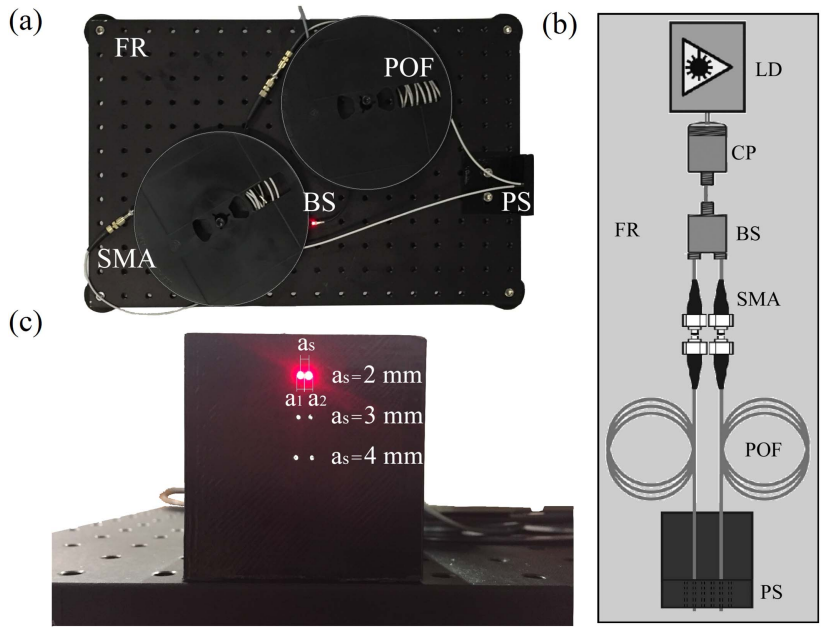

Figure 2. (a) Top picture and (b) scheme of the light source system. LD: laser diode, CP: fibre coupler, BS: beam splitter, SMA: SMA connector, POF: polymer optical fibre, PS: positioner, FR: flat rail. (c) Front picture of the light source equipment.

which case $d = \lambda L/2a_s$. Using this last expression, the following criterion for estimating the angular resolution of an interferometer is defined: two components of a binary system with the same diameter and equal brightness ($f = 1$) will be resolved if the corresponding fringe visibility goes to zero for the longest baseline value ($d_{\max}$) of the interferometer, that is, when the angular separation of the components is equal or bigger than $\lambda/2d_{\max}$ [8].

3. Experimental set-up and procedure

Figure 2 shows a scheme and a picture of the light source system designed for this work. A laser emitting at a wavelength of 650 nm with an output power of 7 mW is split in two beams by means of a beam splitter (BS). These beams are coupled to the SMA connectors of two step-index polymer optical fibres (SI-POF) of 2 m in length (see figure 2(a)). Finally, the free fibre's ends are inserted in two 1 mm-diameter holes located in an L-shape element, named positioner (PS). They are inserted into the back of the PS up to the position where their end faces reach the front face of this element. The PS contains three pairs of holes that are horizontally aligned, with separations of 2, 3 and 4 mm, respectively, from centre to centre (see figure 2(c)). SI-POFs have a large core diameter (∼1 mm) and a high numerical aperture (∼0.5) or large-angle emission cone. 2 m-long SI-POFs are enough to consider the free fibre end faces as uniform and spatially incoherent circular light sources [18, 19], which is necessary in order to use (2), (3) and (4).

The light source system has been designed so that its parameters can be changed in a fast and easy way. On one hand, the use of SMA connectors allows us to change the size of the source without difficulty, just by connecting SI-POFs of different diameters. On the other

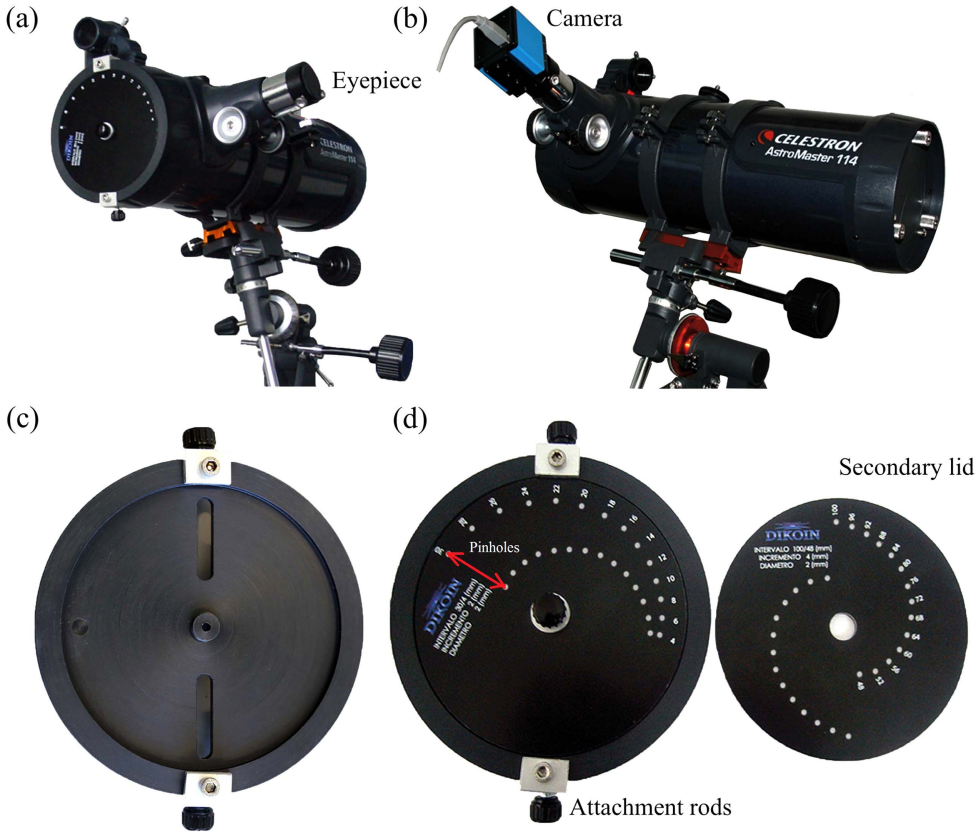

Figure 3. Set-up of the observing equipment. (a) Front picture of the telescope with its aperture blocked by the lid with pinholes. (b) Picture of the telescope with the camera attached to the focal plane. (c) Internal lid. (d) Revolving plate with pinholes locked and not locked in the internal lid. The camera is attached to a laptop through an USB cable allowing direct view of the fringes and the acquisition of images with a variety of electronic gains and exposure times to maximize the image quality.

hand, as it can be seen in figure 2(c), the distance between sources can be changed just by inserting the fibre end faces in a different pair of holes in the L-shape element.

The measurements were carried out in low-light conditions in a corridor located in the basement of our institution. The light source system was placed in front of a telescope at a distance of $L = (54 \pm 1)$ m. The telescope used is the AstroMaster 114 EQ Newtonian with an aperture of 114 mm and a focal length of 1000 mm. Once the telescope is well focused, its aperture is blocked by a lid with several pairs of identical pinholes of 2 mm in diameter separated by different distances from 4 to 30 mm, see figure 3(a). The lid consists of two parts; the internal lid (figure 3(c)), which is locked to the telescope's aperture and the revolving plate containing the pinholes (figure 3(d)). Rotating the revolving plate over the internal lid, the distance d between pinholes can be varied [16], allowing to obtain the interference fringes for different values of d.

The fringes can be observed directly through the telescope's eyepiece. In order to compute the quality of the interference patterns, we acquired digital images or videos of the fringes by means of a camera attached at the focal plane of the telescope (figure 3(b)). We

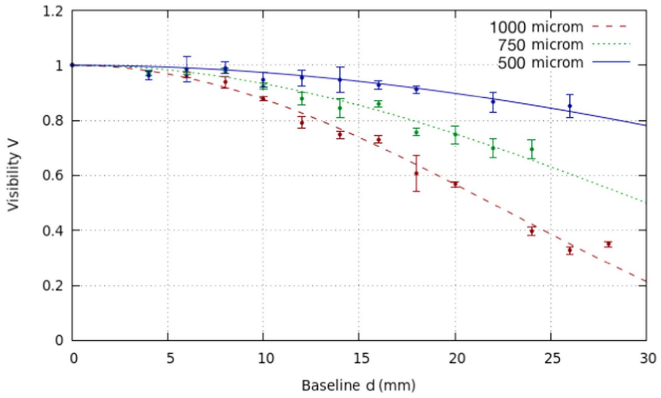

Figure 4. Visibility as a function of the pinhole separation obtained for a single circular source with three different linear diameters. The symbols are the experimental points and the lines are the fittings using (2). $L = 54$ m and $\lambda = 650$ nm.

used a DMK41AU02 commercial camera equipped with the Sony ICX205AL CCD chipset, which is usually employed by amateur astronomers and also in our Aula Espazio Observatory telescopes [20].

This camera has a sensitivity of 0.05 lx (1 lx $=$ 1 lm m^{-2} $=$ 1 cd sr m^{-2}; this value of illuminance is equivalent to the level of light present in a night-scene illuminated under the light of the full moon). This represents the smallest amount of light needed for the camera to produce a video of usable quality at 15–30 frames per second without a telescope. Other characteristics of this camera are a dynamic range of 36 dB, and a pixel size of 4.65 μm. Long exposure times were needed (from 7 s to 10 s) in order to have an appropriate signal-to-noise ratio.

Images were processed by a program implemented in Matlab. This program, after cutting the region of interest, rotating the images and reducing the background noise in each image, provides the photometric cuts of the obtained fringes, from which $I_{\max}$ and $I_{\min}$ can be calculated. For students without programming skills many image analysis softwares are available and a good alternative is ImageJ (https://imagej.nih.gov/ij/) which is freeware, easy to use and able to obtain the photometric cuts of the interference fringes. A photometric cut is the representation of the irradiance levels (or digital number) of all the pixels along any central line crossing the interference fringes perpendicularly, see figure 1. $I_{\max}$ corresponds to the central maximum and $I_{\min}$ to the average of the two adjacent minima. All irradiance measurements were corrected with the background brightness determined by averaging all the irradiance values outside the fringes. For the sake of accuracy, three photometric cuts were calculated for each pinhole separation, and the final visibility value was obtained by averaging the three visibility values corresponding to each photometric cut.

4. Results and discussion

Figure 4 shows the fringe visibility produced by a single fibre as a function of the pinhole separation, for three different fibre diameters: 500 μm, 750 μm and 1000 μm (nominal values). The differences in the magnitudes of the error bars of the visibility values are due to variations of the background light in the corridor where the measurements are carried out. As seen in figure 4, as the fibre diameter increases, the visibility decreases faster and the first

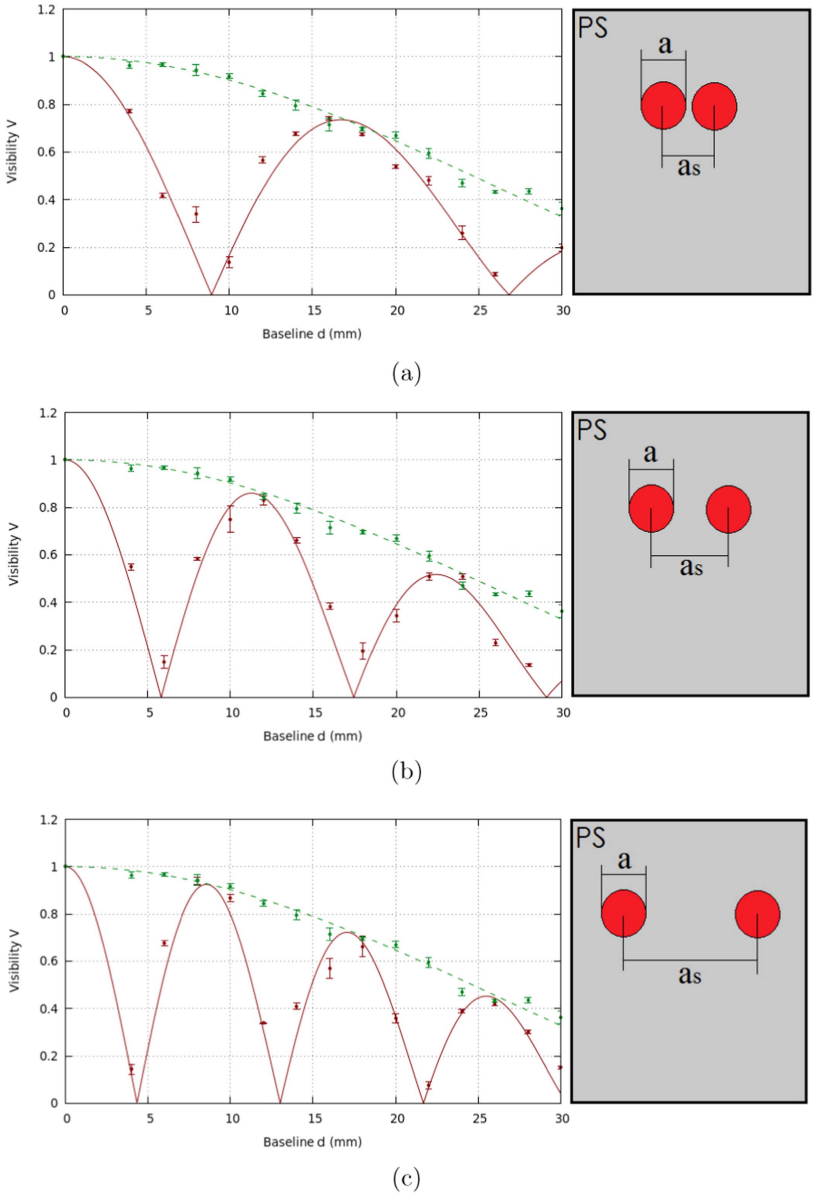

Figure 5. Visibility curve as a function of the pinhole separation obtained for binary circular sources of the same diameter $a = 1000\ \mu$m, with $f = 1$ and $\theta = 0°$, separated by: (a) 2 mm, (b) 3 mm and (c) 4 mm. The circles are experimental points and the solid lines the fittings to (4). The dashed lines and the corresponding points are the fitting to (2) and the experimental points obtained for a single disk of $a = 1000\ \mu$m. $L = 54$ m and $\lambda = 650$ nm.

minimum of the visibility is shifted to smaller baselines. A fit of (2) to the experimental points of each fibre, with $L = 54$ m and $\lambda = 650$ nm, leads to the following results: $a = (510 \pm 30)$ μm, $a = (820 \pm 30)$ μm and $a = (1130 \pm 40)$ μm for each fibre, which differ by 3%, 10% and 13% from their nominal values, respectively.

Table 1. Values of a and a_s obtained from the fittings of (4) to the experimental points corresponding to a double star in figure 5.

Figures	Real a (μm)	Fit a (μm)	Relative error a	Real a_s (mm)	Fit a_s (mm)	Relative error a_s
5(a)	1000 ± 1	990 ± 80	2%	2.0 ± 0.1	1.96 ± 0.05	2%
5(b)	1000 ± 1	1060 ± 70	10%	3.0 ± 0.1	3.02 ± 0.07	6%
5(c)	1000 ± 1	1020 ± 70	5%	4.0 ± 0.1	4.1 ± 0.1	2%

In the following, we show the results obtained by measuring the visibility of the fringes formed by different binary systems. Figure 5 shows the fringe visibility produced by two fibres of the same diameter, namely 1000 μm, oriented parallel to the two pinholes of the lid of the telescope ($\theta = 0°$) and emitting with the same radiance ($f = 1$). Three separation distances between fibres have been used: 2 mm, 3 mm and 4 mm. As it can be seen in the figure, the fringe-visibility curve produced by two fibres is modulated by the visibility curve created by a single fibre. As the distance between fibres a_s increases, the first minimum of the visibility occurs at smaller baselines, and the separations between consecutive minima are shortened. By fitting (4) to the experimental points with $L = 54$ m, $\lambda = 650$ nm, $f = 1$ and $\theta = 0°$, we estimate, for each case, the values of the diameters of the fibres together with their separation. The results obtained are shown in table 1. The experimental measurements carried out with a single fibre of 1000 μm in diameter and their corresponding fittings using (2) have also been included in the figure for each separation distance. The result obtained from these fittings was in all cases $a = 1000 \pm 30$ μm.

As an example, in figure 6 we show the detected interference patterns produced by two identical fibres of $a = 1000$ μm separated by $a_s = 2$ mm, for four different pinhole separation distances: $d = 4$, 6, 10 and 16 mm. The relative brightness profiles of the images and the corresponding theoretical point in the visibility curve for each value of the baseline d have also been represented. It can be noticed that the maxima of the visibility curves get closer to each other as the distance d increases. A similar behaviour occurs in the case of a single source.

In figure 7, we show the strong effect on the visibility curve of the orientation of the two sources with respect to the orientation of the two pinholes on the telescope. We have represented the measurements obtained when the fibres are oriented parallel to the baseline in the telescope ($\theta = 0°$) and when they are oriented perpendicularly ($\theta = 90°$). In both cases, the fibres have the same diameter (1000 μm), they emit the same radiance ($f = 1$) and they are separated by 2 mm. The fittings to the experimental data with (4) have also been represented in figure 7, and the results obtained from the two fittings are shown in table 2. It can also be seen in table 2 that, the value of a_s obtained with $\theta = 90°$ is close to zero, indicating that the two sources oriented perpendicularly to the baseline produce the same visibility curve as that corresponding to a single fibre of the same diameter. The value of the diameter obtained in this case is slightly higher than both the nominal value and the value obtained for $\theta = 0°$. This is the reason why the fitting line of the curve $\theta = 90°$ in figure 7 goes above the fitting line of the curve $\theta = 0°$ in a small range of the baseline distances.

Finally, we have used our light source to simulate the emission of a real binary stellar system, such as Alpha Centauri. This is the closest stellar system to the Solar System, at a distance of 1.34 pc (~4.37 light-years away) [21]. Although the system consists of three stars, we will only take into account the two brightest ones (Alpha Centauri A and B with luminosities $L_A = 1.519 L_\odot$ and $L_B = 0.5002 L_\odot$; where $L_\odot$ is the total luminosity of the Sun

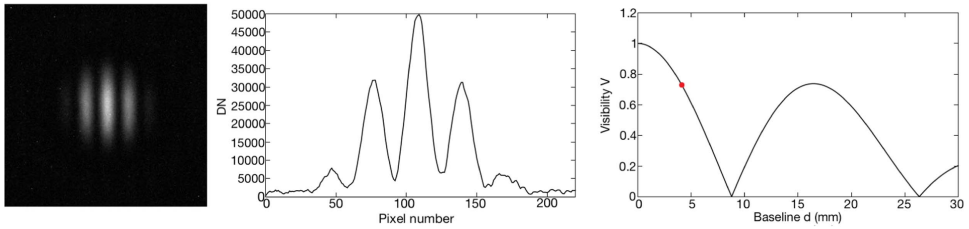

(a) d=4mm

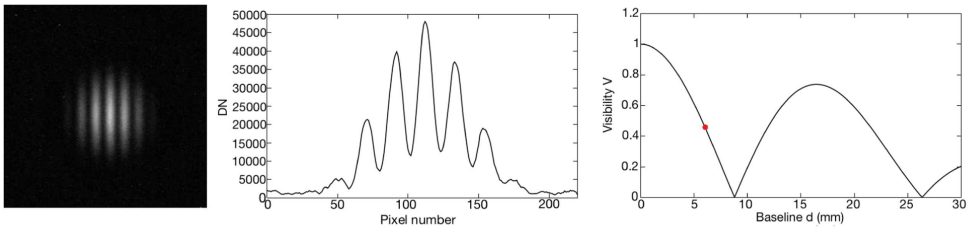

(b) d=6mm

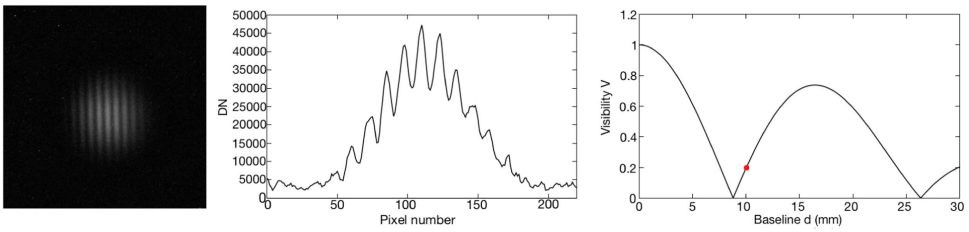

(c) d=10mm

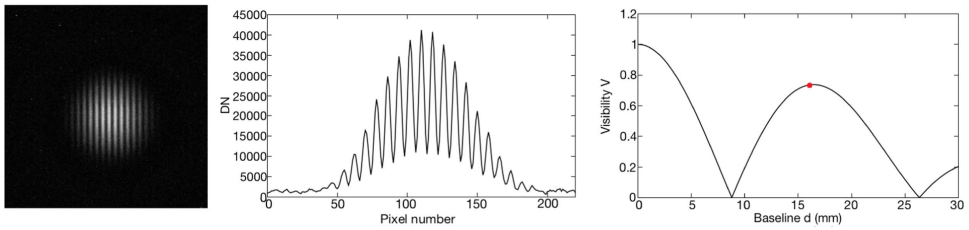

(d) d=16mm

Figure 6. Interference patterns, relative brightness profiles and theoretical point in the visibility curve of images obtained for four different baseline values: 4, 6, 10 and 16 mm. Light source: two fibres of $a = 1000\,\mu$m with $a_s = 2$ mm, $f = 1$, $\theta = 0°$, $L = 54$ m and $\lambda = 650$ nm.

equivalent to 3.828×10^{26} W) [22], neglecting the fainter third component. The ratio between the diameters of Alpha Centauri A and B is 1.42 and their separation varies from 11.2 AU to 35.6 AU (1 AU $= 4.8481 \times 10^{-6}$ pc) [23, 24]. Taking the average value of these two limits, we estimate an average angular separation between stars of $17.16''$ from the Solar System. On the other hand, the contrast of the binary system is estimated assuming that the stars are perfect black body radiators. In that case, the ratio between the total integrated flux received from each component at a wavelength of 650 nm will be,

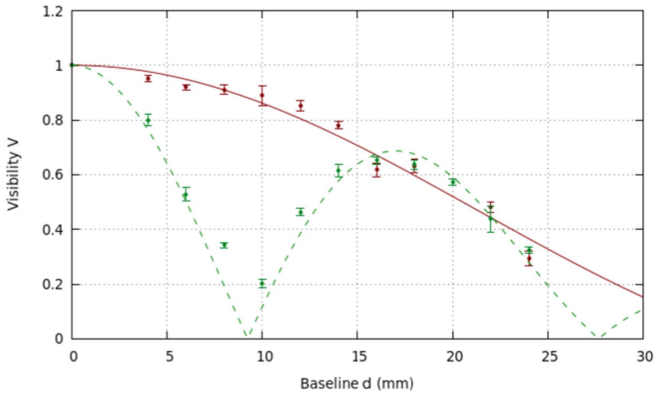

Figure 7. Visibility curves as a function of the pinhole separation obtained for a binary circular source with two different orientations of the pinholes. Dashed line: $\theta = 0°$; Solid line: $\theta = 90°$. Light source: two fibres of $a = 1000\ \mu$m with $a_s = 2$ mm, $f = 1$, $L = 54$ m and $\lambda = 650$ nm.

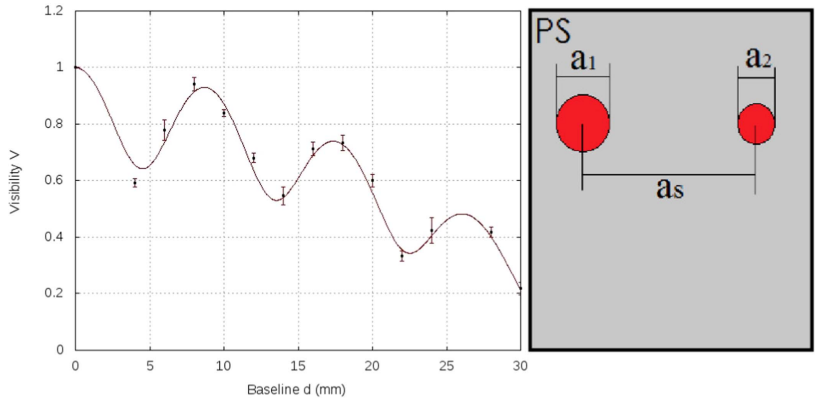

Figure 8. Visibility curve corresponding to the experiment replicating the characteristics of the Alpha Centauri system. Symbols represent the experimental data and the line is the fitting to the data using (3).

Table 2. Values of a and a_s obtained from the fittings of (4) to the experimental points corresponding to a double star in figure 7 oriented parallel and perpendicular to the baseline in the telescope.

θ (°)	Real a (μm)	Fit a (μm)	Relative error a	Real a_s (mm)	Fit a_s (mm)	Relative error a_s
90	1000 ± 1	1220 ± 300	21%	2.0 ± 0.1	0.01 ± 0.02	—
0	1000 ± 1	1000 ± 100	0%	2.0 ± 0.1	1.95 ± 0.05	3%

Table 3. Values of a_1, a_2, a_s and f obtained from the fittings of (3) to the experimental points corresponding to a double star in figure 8.

	a_1 (μm)	a_2 (μm)	a_s (mm)	f
Real	1000 ± 1	750 ± 1	4.0 ± 0.1	0.27 ± 0.05
Fit	1000 ± 200	730 ± 70	4.0 ± 0.1	0.22 ± 0.04
Relative error	3%	3%	1%	18%

$$f = \frac{f_2}{f_1} = \frac{B_\lambda(T_B)}{B_\lambda(T_A)} \cdot \left(\frac{R_B}{R_A}\right)^2 = 0.37 \tag{5}$$

where $B_\lambda(T)$ is the spectral radiance emitted by a black body of temperature T described by Planck's law, R_A and R_B the radii of each component, and $T_A = 5790$ K and $T_B = 5260$ K their temperatures [22]. Students can examine the behaviour of the Planck law on (5) in educational websites [25].

We simulate this stellar system using two fibres of diameters $a_1 = 1000$ μm and $a_2 = 750$ μm, giving a ratio of $a_1/a_2 = 1.31$, and separated by $a_s = 4$ mm, which corresponds to an angular distance of 15″ from the telescope. Regarding the contrast of the simulated binary star, the closest value to the real contrast of 0.37 that we could obtain in our experiments was $f = 0.27 \pm 0.05$. This value was achieved by covering the end face of one of the fibres with an adequate absorptive filter. The visibility curve obtained with our designed source and its fitting using (3) can be seen in figure 8. It can be noticed that the amplitude of the visibility curve decreases owing to the decrease of the contrast. The results of the fitting can be seen in table 3. A very good agreement between the real data and the experimental results has been obtained, with relative errors equal or less than 18%.

5. Summary and conclusions

We have used a simple experimental set-up that recreates the operation of the Michelson stellar interferometer to explore the capabilities of such an instrument, as well as the physical properties of binary light sources. The emission pattern of double stellar sources has been reproduced by using two 2 m-long POFs illuminated by a laser, which produce closely located circular, uniform, quasi-monochromatic and spatially incoherent emission patterns. Using this method, diameters and separations of different sources placed at 54 m from the interferometer have been determined with relative errors less than 16%. Information about the relative orientation of the light sources can also be retrieved by introducing an additional parameter, θ, to be fitted in (3).

In our experiments we have come to resolve angular widths of around 2″. These widths could have been resolved just by direct observation with our telescope/CCD system (without any lid) since the limit of diffraction of the telescope is 1.4″ and the angular coverage of each CCD pixel is 0.95″. The angular resolution limit of our interferometer is 0.6″, given that the maximum distance between the pinholes, $d_{\max}$, is smaller than the aperture of the telescope. Nevertheless, it must be taken into account that the objective of our demonstration is not to show how the interferometry can beat the Rayleigh resolution limit of the telescope but to demonstrate a simple operation of the stellar interferometer with double star systems. The smallest size measured with our interferometer, 2″, is comparable to Uranus (3.7″) and Neptune (2.2″). Furthermore, we were able to distinguish and deduce the contrast between the

components of a binary system that recreates the conditions of the Alpha Centauri system with sources separated an angular distance of 15″.

5.1. Implications for other teaching courses

The simplicity of the experimental device and the satisfactory results obtained make this experiment ideal to be implemented in postgraduate astrophysics, astronomy or optics subjects. On the one hand, it implies the use of a telescope, a digital camera, and image processing tools. On the other hand, it provides the hands-on experience needed to understand the basic concepts of interferometry underlying the experiment. For introductory students, or only marginally addressing this subject, the experiment can be also carried out avoiding the image processing and the non-linear fitting, just finding the smallest value of the pinhole separation for which the interference fringes disappear. For advanced students coursing different subjects from optics to astronomy or image analysis, the experiment can be fully replicated as it has been carried out over the last years in our university. Specifically, this experiment has been regularly performed by students of the Master in Space Science and Technology. The initial feeling of the students is the astonishing nature of the demonstration of interference that results in a positive enthusiasm to execute a real experiment on a subject that is typically explained from a distant theoretical position. Most practical difficulties are linked to the use of a real telescope and the analysis of the images. The experiment is highly complementary with other subjects in this masters course, such as: *Optics*, *Astronomy and Astrophysics* or *Astronomical and Space Signal Processing* [20].

Finally, it is important to highlight that, even with the didactic nature of the experiment here presented, the physical principles underlying our simple interferometer and a real astronomic one are the same. The interferometer we show can be easily adapted to a real astronomical measurement. The angular separation of real binary stellar systems could be measured with any 30–50 cm telescope available in many university departments of astronomy. The telescope may have to be masked similarly to the device here presented, but bigger pinhole diameters and longer exposure times would be required in order to obtain high enough irradiance levels, as well as the use of a narrow band filter to capture monochromatic light.

Acknowledgments

This work has been supported by the following institutions: Diputacin Foral de Bizkaia/Bizkaiko Foru Aldundia through the Aula Espazio Gela, Ministerio de Economia y Competitividad under projects TEC2015-638263-C03-1-R and AYA2015-65041-P (MINECO/FEDER, UE), Gobierno Vasco/Eusko Jaurlaritza under projects IT933-16 and IT-765-13 and ELKARTEK (KK-2016/0030 and KK-2016/0059) and by the University of the Basque Country (UPV/EHU) through programs UFI11/16 and UFI11/55. We thank Raul Cosgaya, from the Department of Mechanical Engineering, for preparing the L-shape element.

References

[1] Hecht E and Zajac A 2003 *Optics* 4th edn (San Francisco, CA: Addison Wesley)
[2] Tyson R 2010 *Principles of Adaptative Optics* 3rd edn (Boca Raton, FL: CRC Press)
[3] Law N M, Mackay C D and Baldwin J E 2005 Lucky imaging: high angular resolution imaging in the visible from the ground *Astron. Astrophys.* **446** 739–45

[4] Mendikoa I, Sánchez-Lavega A, Pérez-Hoyos S, Hueso R, Rojas J F, Aceituno J, Aceituno F J, Murga G, de Bilbao L and García-Melendo E 2016 PlanetCam UPV/EHU: a two channel lucky imaging camera for Solar System studies in the spectral range 0.38-1.7 mm *Astron. Soc. Pacific* **128** 22
[5] Wolf E 2007 *Introduction to the Theory of Coherence and Polarization of Light* 1st edn (Cambridge: Cambridge University press)
[6] Michelson A A and Pease F G 1921 Measurement of the diameter of Alpha Orionis with the interferometer *Astrophys. J.* **53** 249–59
[7] Monnier J D 2003 Optical interferometry in astronomy *Rep. Prog. Phys.* **66** 789–857
[8] Glindemann A 2011 *Principles of Stellar Interferometry* (Heidelberg: Springer)
[9] Glindemann A Introduction to spatial interferometry (available at: https://eso.org/sci/facilities/paranal/telescopes/vlti/tuto/tutorial_spatial_interferometry.pdf)
[10] Haniiff C 2007 An introduction to the theory of interferometry *New Astron.* **51** 565–75
[11] Pryor M J 1959 Measuring artificial star separation by interference *Am. J. Phys.* **27** 101–3
[12] Sharpe J P and Collins D A 2011 Demonstration of optical spatial coherence using a variable width source *Am. J. Phys.* **79** 554–7
[13] Koda J, Barrett J, Shafto G and Slechta J 2016 A Michelson-type radio interferometer for university education *Am. J. Phys.* **84** 249–56
[14] Fendley J J 1982 Measurement of refractive index using a Michelson interferometer *Phys. Educ.* **17** 209–11
[15] Libbrecht K G and Black E D 2014 A basic Michelson laser interferometer for the undergraduate teaching laboratory demonstrating picometer sensitivity *Am. J. Phys.* **83** 409–17
[16] Illarramendi M A, Hueso R, Zubia J, Aldabaldetreku G, Durana G and Sánchez-Lavega A 2014 A daylight experiment for teaching stellar interferometry *Am. J. Phys.* **82** 649–53
[17] Berger J P and Segransan D 2007 An introduction to visibility modeling *New Astron.* **51** 576–82
[18] Yoshimura H, Asakura T and Takai N 1992 Spatial coherence properties of light from optical fibers *Opt. Quantum Electron.* **24** 631–46
[19] Imai M and Ohtsuka Y 1982 Spatial coherence of laser light propagating in an optical fiber *Opt. Quantum Electron.* **14** 515–23
[20] Sánchez-Lavega A, Pérez-Hoyos S, Hueso R, del Rio-Gaztelurrutia T and Oleaga A 2014 The Aula Espazio Gela and the master of space science and technology in the Universidad del País Vasco (University of the Basque Country) *Eur. J. Eng. Educ.* **39:5** 518–26
[21] Wilkinson J 2012 The sun and stars *New Eyes on the Sun* (*Astronomers' Universe*) (Heidelberg: Springer) pp 219–36
[22] Thévenin F, Provost J, Morel P, Berthomieu G, Bouchy F and Carrier F 2002 Asteroseismology and calibration of Alpha Cen binary system *Astron. Astrophys.* **392** L9–12
[23] Kervella P, Thévenin F, Ségransan D, Berthomieu G, Lopez B, More P and Provost J 2003 The diameters of α Centauri A and B *Astron. Astrophys* **404** 1087–97
[24] Hartkopf W and Mason D M 2008 *Sixth Catalog of Orbits of Visual Binaries* (US Naval Observatory)
[25] https://astrogeology.usgs.gov/tools/thermal-radiance-calculator/